Available online at www.sciencedirect.com
SCIENCE DIRECT®
Bioelectrochemistry 62 (2004) 83–93
Bioelectrochemistry
www.elsevier.com/locate/bioelechem

Electroporation of subcutaneous mouse tumors by rectangular and trapezium high voltage pulses

U. Pliquett[a], R. Elez[b,c], A. Piiper[b,c], E. Neumann[a,*]

[a] Physical and Biophysical Chemistry, Faculty of Chemistry, University of Bielefeld, P.O. Box 100 131, D-33501 Bielefeld, Germany
[b] Department of Internal Medicine, Johann Wolfgang Goethe-University, D-60590 Frankfurt, Germany
[c] Department of Internal Medicine II, Molecular Oncology Unit, University of Saarland, D-66422 Homburg/Saar, Germany

Received 17 March 2003; received in revised form 1 August 2003; accepted 26 November 2003

Abstract

The artificial electrotransfer of bioactive agents such as drugs, peptides or therapeutical nucleic acids and oligonucleotides by membrane electroporation (MEP) into single cells and tissue cells requires knowledge of the optimum ranges of the voltage, pulse duration and frequency of the applied pulses. For clinical use, the classical electroporators appear to necessitate some tissue specific presetting of the pulse parameters at the high voltage generator, before the actual therapeutic pulsing is applied. The optimum pulse parameters may be derived from the kinetic normal mode analysis of the current relaxations due to a voltage step (rectangular pulse). Here, the novel method of trapezium test pulses is proposed to rapidly assess the current (I)/voltage (U) characteristics (IUC). The analysis yields practical values for the voltage U_{app} between a given electrode distance and pulse duration t_E of rectangular high voltage (HV) pulses, to be preset for an effective in vivo electroporation of mouse subcutaneous tumors, clamped between two planar plate electrodes of stainless steel. The IUC of the trapezium pulse compares well with the IUC of rectangular pulses of increasing amplitudes. The trapezium pulse phase (s) of constant voltage and 3 ms duration, following the rising ramp phase (r), yields a current relaxation which is similar to the current relaxation during a rectangular pulse of similar duration. The fit of the current relaxation of the trapezium phase (s) to an exponential function and the IUC can be used to estimate the maximum current at a given voltage. The IUC of the falling edge (phase f) of the trapezium pulse serves to estimate the minimum voltage for the exploration of the long-lived electroporation membrane states with consecutive low-voltage (LV) pulses of longer duration, to eventually enhance electrophoretic uptake of ionic substances, initiated by the preceding HV pulses.

Keywords: Electroporation; Skin tumor; Trapezium pulse; Preset parameters

1. Introduction

High voltage pulses have traditionally been used to transfer bioactive substances such as drugs, therapeutical peptides and nucleic acids or oligonucleotides into cells by the method of membrane electroporation (MEP) [1,2]. The controlled drug delivery by MEP gains increasing importance not only in cell biology and biotechnology but also for novel clinical applications in electrochemotherapy [3–5] and delivery of nucleic acids using electroporation in vivo. It is well known that electroporative high voltage pulses greatly increase the transdermal drug transport improving the pharmacological potential of drug delivery [6]. The practical aspects of the electrotransfer methods comprise the determination of optimum ranges for the pulse voltage and the pulse time, as well as the number of pulses [7]. In particular, the clinical use of classical electroporators appears to necessitate the presetting of the pulse parameters before the actual therapeutic pulsing is applied.

The mechanism of membrane electroporation (MEP) and of the various electroporative processes are slowly being understood in physicochemical terms [1,6,8–14]. In brief, when biological cells, organelles or lipid vesicles are subjected to short-lasting (100 μs–10 ms) electric field pulses, the (ionic) Maxwell–Wagner polarization of the cell membranes enormously increases the membrane potential difference. The electrically induced membrane field, $E_{ind} = -\Delta\varphi_{ind}/d_m$, where $\Delta\varphi_{ind}$ is the induced transmembrane potential and $d_m = 5$ nm is the assumed membrane thickness, can be orders of magnitude larger than the

* Corresponding author. Tel.: +49-521-106-2053; fax: +49-521-106-2981.
E-mail address: eberhard.neumann@uni-bielefeld.de (E. Neumann).

1567-5394/$ - see front matter © 2004 Elsevier B.V. All rights reserved.
doi:10.1016/j.bioelechem.2003.11.001

externally applied field strength $E_{app} = U_{app}/\ell$, where U_{app} is the voltage applied and ℓ is the electrode distance.

The stationary value of the induced contribution E_{ind} at the pole caps of spherical and ellipsoidal cells can be specified in line with the relationships derived previously [15]. In modern terminology, the expression:

$$E_{ind} = \frac{-\Delta\varphi_{ind}}{d_m} = F\frac{a}{d_m} f_\lambda E \quad (1)$$

appears to be most useful, where F is the geometrical shape factor (for spheres $F = 1.5$) and the ratio a/d_m the geometrical amplification factor. For cells of radius $a = 5$ μm, a/d_m is as large as 1.5×10^3. If the membrane conductivity κ_m is small compared to both the cell interior κ_{in}, the exterior medium κ_{ex}, the condition $a \gg d_m$ for cells and organelles specifies the conductivity factor to [1]:

$$f_\lambda = 1 - \kappa_m \frac{a(\kappa_{ex} + 0.5\kappa_{in})}{d_m \kappa_{ex} \kappa_{in}} \quad (2)$$

For many biotechnological applications, where $\kappa_{in} \gg \kappa_{ex}$ holds, the expression $f_\lambda = 1 - 0.5(\kappa_m/\kappa_{ex})(a/d_m)$ can be used. For densely packed cells [9] and for bacterial rods of length $2a$ the approximation $E_{ind} = (a/d_m) f_\lambda E$ may be applied for the pole caps. Since all living cells exhibit a natural membrane potential $\Delta\varphi_{nat} = \varphi_{in} - \varphi_{ex}$, where φ_{in} is the electric potential of the cell interior, and $\varphi_{ex} = 0$ is the extracellular potential commonly used as zero reference; typically, $\Delta\varphi_{nat} = -70$ mV.

The total transmembrane potential $\Delta\varphi_m(\theta)$ at the angular position θ relative to the direction of the external field (x-direction) through the midpoint of the cell is given by the sphere approximation [1]:

$$\Delta\varphi_m(\theta) = -\left[\frac{3}{2} a f_\lambda E + \frac{\Delta\varphi_{nat}}{\cos\theta}\right] |\cos\theta| \quad (3)$$

The corresponding membrane field is $E_m(\theta) = E_{ind}(\theta) + E_{nat}$, where the contribution of $E_{nat} = (-\Delta\varphi/d_m)\,|\cos\theta|/\cos\theta$ to E_m in the direction of x is asymmetric. At the left pole cap ($\cos\theta = -1$), $E_m > E_{nat}$ and at the right pole cap ($\cos\theta = 1$), $E_m < E_{nat}$. For elongated bacteria of length $2a$ or for densely packed cells, the approximation $F = 1$ in Eq. (1) is appropriate. It is well known that the change in the membrane field E_m (or of the natural field E_{nat}) can cause structural changes in the membrane phase. In lipid bilayers, the enhanced field E_m may enlarge the conducting aqueous pathways or pores [8,16,17] for smaller ions and larger ionic or polar molecules. The lipid rearrangements involved in pore formation are the structural basis for the electroporative transport. At moderate field strengths, $E \leq 1 \pm 0.5$ kV/cm for cells of radius $a = 5$ μm and pulse durations $t_E \leq 10$ ms, pore formation and resealing appear reversible; the resistance recovers completely [18].

At higher field strengths and larger pulse durations, isolated cells, tissue cells and cell aggregates exhibit irreversible changes. Specifically, the corneocytes of the stratum corneum (SC) appear to reorganize smaller pores into localized transport regions (LTR) which at higher field strengths reseal only extremely slowly [19]. Proper pore resealing after pulse applications is required for the survival of cells. Irreversible damage and local cell death in a part of the tissue or of cell aggregate may be tolerable in electrochemotherapy (ECT) of tumors. In direct gene transfer therapies, side effects of cell damage must be minimized. Technically, this means that intensity and duration of the therapeutic pulses must be adjusted to optimum values, requiring some previous knowledge of the electrical properties of the cell membranes and the tissue as a whole.

The primary aim for therapeutic applications is to explore the electrical conditions already before the therapeutic high voltage pulses are applied. In using present electroporator devices, proper presetting of the pulse duration appears necessary.

Here, a procedure is proposed to obtain the presetting parameters from a special double ramp pulse, in the form of a trapezium, applied shortly before the actual electroporative high voltage pulsing is performed. The detailed outline of the trapezium procedure aims at a practical guidance to obtain the voltage and time parameters for the presetting. The usefulness of this approach is judged from a comparison of the trapezium ramp data with the results of the analysis of current relaxations due to voltage steps (rectangular pulses).

In many cases, the high field-induced electrical changes of cells can be satisfactorily modeled with electric equivalent circuits (see Fig. 1). In the simplest case, the cell interior is represented as a conductive medium of resistance R_i and of conductivity $\kappa_{in} = 1.4$ S/m (muscle cells), surrounded by a practically nonconductive membrane of resistance R_m and capacitance C_m. The rest of the system is represented by the extracellular medium in between the cells with the resistance R_a. For instance, when MEP creates ionic pathways in SC, the membrane resistance R_m drastically decreases during the pulse time and increases again after the pulse termination [20]. It is the time course of $R_m(t)$ which can be subjected to physicochemical analysis.

Model studies with isolated cells [16] and lipid bilayer vesicles [21] have shown that MEP and the transport through the electroporated membrane surface patches are highly localized. Net-transport like small-ion exchange appears only at a critical pore density where, at constant overall pore surface, transport pores must develop [14]. In a multi-layered system, such as the SC, the larger small-ion transport pores reorganize to LTR for the electrophoretic passage of larger poly-ionic molecules [22]. The critical pore density occurs in a critical range of the membrane field strength and is dependent on the pulse time [18]. Many actually measured uptake curves reflect not only the extent of MEP and transport during the pulse time but also the after-field transport of the pore

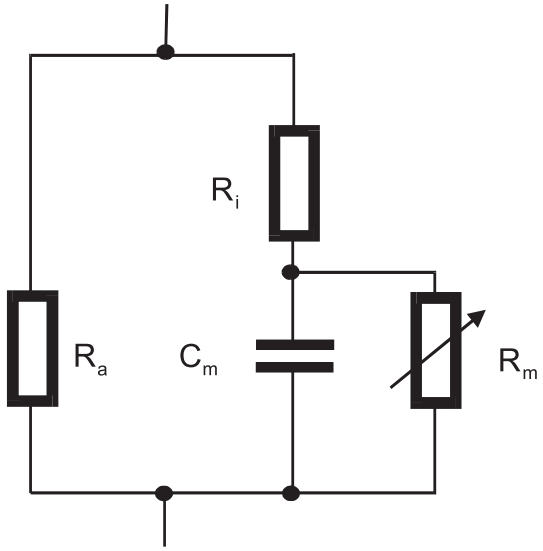

Fig. 1. Simple electrical equivalent circuit (EEC) for a tissue cell. R_m and C_m model the resistance and the capacitance of the cell membranes, respectively, and R_a and R_i are the resistances of the extracellular and the intracellular parts, respectively. When conductive electropores are induced by high voltage pulses, R_m is a time-variable resistance.

resealing phase because of the longevity of transport pores [1,10].

In the case of the field-dependent and time-dependent transport curves (electropermeabilization curves), it has been instrumental to operationally define a critical midpoint (or half-maximum) field strength $\bar{E}_c = \bar{U}_c/\ell$ of the critical transport range $\bar{E}_c \pm \Delta E_c$ or $\bar{U}_c \pm \Delta U_c$ of the cell population [23,24]. Usually, $\bar{E}_c$ increases with decreasing pulse time t_E [10,11,18]. The details mentioned so far are a part of the specific basis for the objective to provide a practical guidance for presetting high voltage generators in cell biological and medical applications of the electroporation technique.

2. Materials and methods

2.1. Tumors

A549 human tumors have been subcutaneously implanted at both sides of the back of NMRI nude mice and have been grown for 2 weeks. Before the pulse experiments, the mice have been anesthetized with isofluorane and clamped into a mouse holder, such that the tumor is easily accessible for the two parallel, stainless steel plate electrodes (8×6 mm^2) with integrated inner electrodes to measure the inner voltage U. The distance between the integrated inner electrodes is the same as the distance between the outer electrodes. The electrode surface facing the tumor has been covered with conductive paste. In Fig. 2, the schematic cross section shows the main features of a typical mouse tumor in a skin fold, clamped between the two planar metal electrodes. In order to calculate the electric field distribution between the electrodes across the tumor, the various tissue thicknesses are indicated. Fig. 3 visualizes the inhomogeneous field distribution (A) and the corresponding electric potential profile (B) and voltages across the various parts, specified in the figure legend. It is readily seen that it is the skin which represents the part of highest ionic resistance due to its outer SC layer. The skin as a whole consists of the thin SC of thickness $d_{SC} = 15 \pm 5$ μm and several other layers of higher conductivities. The simulation data shown in Fig. 3 refer to the skin as a whole of overall conductivity $\kappa(\text{skin}) = 20$ mS/m.

2.2. Apparatus

The high voltage ($U_{app} \leq 1$ kV) is generated by using a specially developed arbitrary function generator (Scientopo-

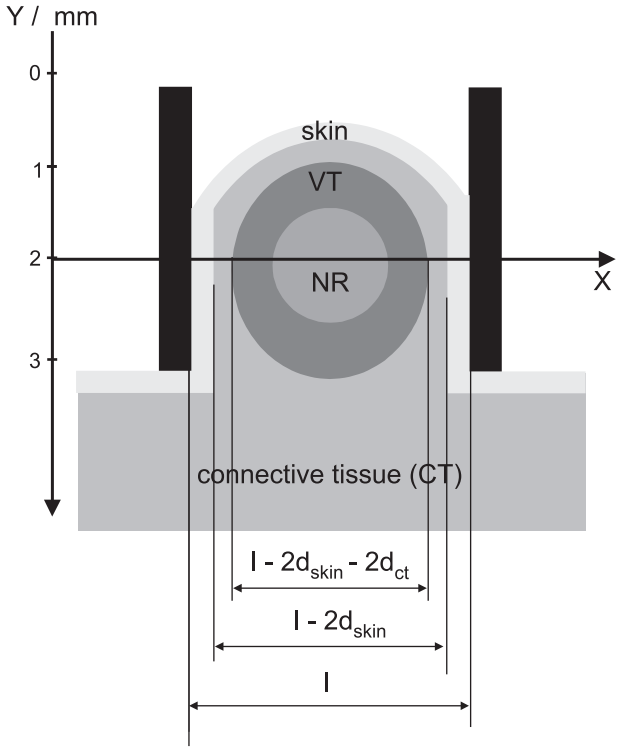

Fig. 2. Schematic cross section of a typical subcutaneous mouse tumor (xenographed with A549 cells) designed according to a stained cross section obtained after electroporative transfer of oligonucleotides [25]. The tumor is clamped between the two metal electrodes (black) of a special holding device, in which the mouse is gently fixed (below the holder). The electrodes of (polished) stainless steel for the applied voltage U_{app} are equipped with smaller inner electrodes of gilded cooper. The measured voltage is the inner voltage $U = U_{app}$-2 U_{ES} ($< U_{app}$). This setup avoids the electrode polarization contributions U_{ES} at the two current supply electrodes. The distance ℓ between the inner electrodes is the same as that between the outer electrodes (U_{app}). The skin covering the tumor has here the thickness $d_{skin} = 0.4$ mm and includes the stratum corneum layer of thickness $d_{SC} = 15 \pm 5$ μm; CT, connective tissue of thickness $d_{CT} = 1 \pm 0.5$ mm; NR, the necrotic region of thickness $d_{NR} = 2 \pm 1$ mm; VT, vital region of the tumor with a thickness of $d_{VT} = 0.5 \pm 0.2$ mm. The mouse tumors used here have localized, non-distributed, necrotic regions as judged from the stained cross sections obtained after successful oligonucleotide transfer [25].

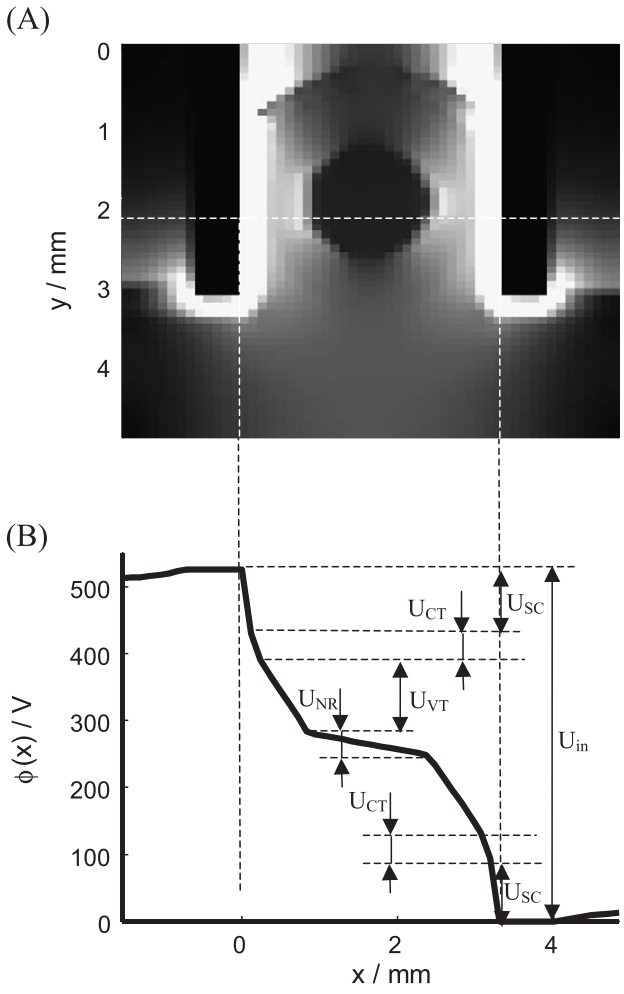

Fig. 3. Cross section of the electrode tumor system (A) for the calculations of the electric field distribution and (B) the electric potential profile ϕ(x) of a mouse subcutaneous tumor in a skin fold, clamped between planar stainless steel electrodes (ES) at a distance of $\ell = 3.2$ mm. The electric potential profile refers to the height y = 2 mm and the voltage is U = 526 V. The cross section has the same dimension as that in Fig. 2 (bitmap of Fig. 2). The gray contrast image of the E-distributions is continuous between the high-field area (white) of E = 9.6 kV/cm and the low field area (black) of E = 0. The numerical values of the various voltages U_{SC}, U_{CT}, U_{VT}, U_{NR}, respectively, are calculated using known average conductivity values, measured on isolated specimen of mouse skin, of CT, VT and NR (during the presence of high voltages): κ (ES) = 0.1 MS/m, κ (CT) = 0.08 S/m, κ (VT) = 0.1 S/m, κ (NR) = 0.6 S/m and κ (air) = 1 μS/m. The value κ (skin) = 20 mS/m refers to the skin of thickness d_{skin} as a whole, consisting of SC of thickness d_{SC} and other layers.

rator) [24], containing a time-domain based impedance meter. Both, the voltages U_{app} at the outer electrodes (pulse application) and U at the inner electrodes are recorded by a digital oscilloscope (TDS 540C, Tektronix, Beaverton, OR, USA). The voltage trace at the outer electrodes only serves as a monitor for the correct pulse application while the voltage U across the inner electrodes is used for further data processing. The total current $I(t)$ is recorded with a current transducer attached to the oscilloscope.

The shapes of the applied voltage pulses are either rectangular or a trapezium-shaped double ramp. If the amplitudes of the resulting currents $I(t)$ are nonlinearly dependent on the voltage, they presumably indicate structural changes of the object between the electrodes. Because of the potential drop ($\Delta\varphi_{ES}$) at the electrodes, which is dependent on the current density, the voltage U at the inner electrodes decreases with time (up to 10%) compared to the constant voltage applied U_{app}.

A simplified version of the Scientoporator has been used to introduce antisense oligodesoxy-nucleotides into the interior of tumors by in vivo MEP [25]. Once the cell constant $z = A_{eff}/\ell_{eff}$ of the electrode configuration is determined, the conductivity $\kappa = G/z$ is calculated from the conductance $G = I/U$, where A_{eff} and ℓ_{eff} are the effective electrode surface and distance, respectively. For linear, time-invariant objects the conductance $G = I/U$ is constant (ohmic behavior). If the stationary current changes nonlinearly with U, the differential (or dynamic) conductance $G_D = dI/dU$ is used to obtain closed analytical expressions. For most practical cases, the simple ratios $G = I/U$ are, however, sufficient to describe the nonlinear current dependence on voltage.

3. Results

The time courses of the measured signals (e.g., Fig. 4), $I(t)$ and $U(t)$, contain resistive and capacitive contributions, which can be specified in terms of individual circuit

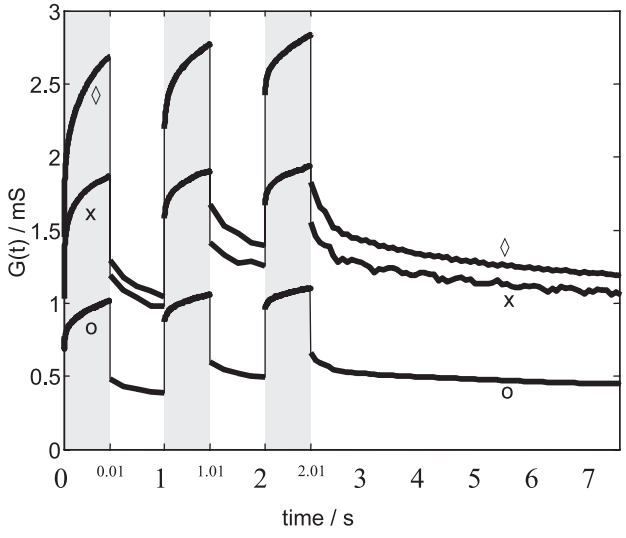

Fig. 4. Time course of the conductance G(t) = I(t)/U at constant voltage U during $t_E = 10$ ms pulse duration for 3 representative field strengths E = U/ℓ, (○) 71.8 V/cm ($U_{app} = 50$ V), (x) 131.3 V/cm ($U_{app} = 100$ V), (◇) 160.2 V/cm ($U_{app} = 150$ V), for three consecutive pulses (at given E) at a 1 s interval between the pulses, respectively. The shaded areas refer to the pulse duration t_E = 10 ms, here stretched with respect to the t/s scale. The dc-conductance prior to pulsing is slightly different for each tumor; it is, however, always in the range $G_0 = 0.1 \pm 0.05$ mS. The different tumors (n = 5 for 5 different voltages) used are of the same type as those sketched in Fig. 2., but are all one week older.

elements. Impedance spectroscopy of the mouse tumors before the pulsing (at $E=0$) yields the average values of $R_a = 15.7 \pm 7.8$ kΩ, $R_i = 363 \pm 100$ Ω, $C_m = 31.8 \pm 14.8$ nF (Fig. 1). If there are structural changes such as MEP, these quantities change in the presence of a field pulse and continue to change after field application. Note that the relatively large standard deviations of the impedance refer to the differences of the tumors at low measuring voltage. The actual time-courses in the presence of high electric fields can be represented as relative changes and are thus only marginally affected by the low-field impedance data.

3.1. Conductance relaxations at constant U_{app}

In Fig. 4, it is seen that the conductance at consecutive rectangular voltage pulses, applied for $t_E = 10$ ms in intervals of $\Delta t = 1$ s, first rapidly increases with time, followed by a slower increase. After switching off the voltage, there is first a rapid decrease, corresponding to the previous rapid in-field increase, followed by several slower phases. For demonstration, three typical voltages are selected. The conductances increase with voltage and pulse number. In Fig. 5, it is shown that the dc-resistance decreases during the pulse and increases again after the pulse. Qualitatively, the increase in the resistance is consistent with the resealing of pores and tissue reorganization (mostly of the SC). Because of the large resistance of the SC the respective field strength $E_{SC} = U_{SC}/d_{SC}$ is high (Fig. 3B). Therefore, the observed resistance changes dominantly originate from the SC. Note that the skin conductivity (20 mS/m) is a (measured) mean value. See the legend to Fig. 3. From the database of the electroporative transfer of oligonucleotides [25] it is concluded that, once the SC is permeabilized, the rest of the tumor is electroporated, too.

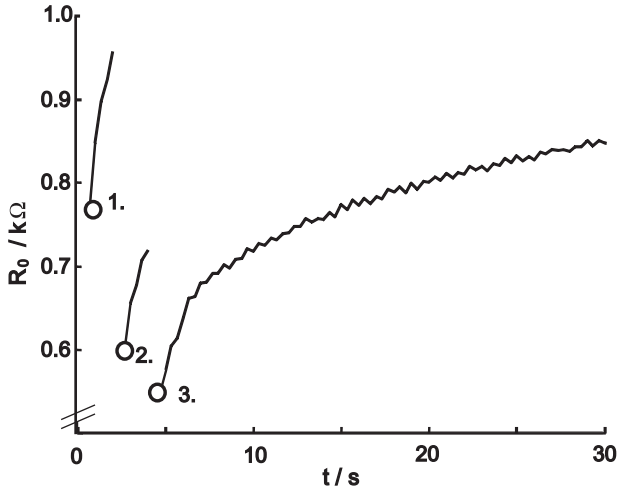

Fig. 5. Recovery of the tissue resistance of a tumor (n = 1) after high voltage pulses: DC resistance R_0 ($t \gg t_E$) as a function of time, after three consecutive rectangular pulses have been applied, starting at the time points t = 0, 2 and 4 s, indicated by the circles (○): $U_{app} = 100$ V ($\ell = 0.7$ cm) or E = 131 V/cm and $t_E = 10$ ms; initial resistance R_0 (t = 0) = 12.2 kΩ.

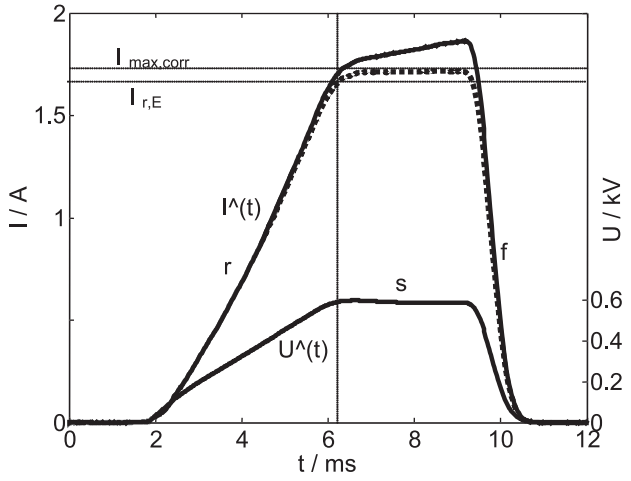

Fig. 6. Time course of the current I(t) as a response to a trapezium-shaped voltage pulse U(t), applied to a single mouse tumor (n = 1) at electrode distance $\ell = 0.7$ cm. (r), rising edge with slope $m_{u,r} = \Delta U/\Delta t_1 = 150$ kV/s up to the time point t = 4 ms; (s) stationary phase at $U_S = 600$ V lasting for $\Delta t_S = 3.3$ ms, recorded as dashed line; (f) falling edge of voltage slope $m_{u,f} = \Delta U_3 / \Delta t_3 = -500$ kV/s, for $t > t_S =$ 7.3 ms, where $\Delta t_f = 1.2$ ms. The estimate of $I_{r,E} = 1.7$ A refers to the onset of the stationary phase (s). The dashed line refers to the Eq. (12) of the text, representing the corrected current without the Joule heating contribution, heading at $I_{max,corr} = 1.75$ A. The conductance before pulsing is $G_0 = 54.3$ μS.- The actual time course represents one example out of n = 15 tumors.

The actual current traces $I(t) = G(t)U$ are readily reproduced from the $G(t)$ curves. The (subtracted) rapid initial contributions of the capacitive elements are quantified by the impedance data. It is interesting to note that the current traces obtained for tissue like liver with needle electrodes are very similar (data not shown) to the current traces of tumors clamped between stainless steel plate electrodes as in Fig. 2.

3.2. Trapezium voltage pulse

As seen in Fig. 6, a trapezium-shaped voltage pulse (double ramp), $U^{\wedge}(t)$, causes a roughly trapezium-shaped current pulse $I^{\wedge}(t)$. Three ranges are distinguished: the rising phase (r), the stationary voltage phase (s) and the decay phase (f). Because Joule heating causes an increase in the conductance with time, the data analysis requires a correction for the Joule heating contribution such that the calculated current level $I_{max,corr}$ is a key parameter for the data analysis; see below. In order to cover the voltage range (between 50 and 500 V), known to effectively electroporate tissue of thickness $\ell \leq 1$ cm [25] with rectangular pulses of up to 10 ms duration, the maximum trapezium voltage of 600 V has been chosen. In the voltage range up to 300 V, the measured current density does not exceed 1 A/cm^2 because of the high resistance of the SC. For $U \leq 300$ V, straightforward simulation shows that Joule heating is negligibly small for pulse durations of ≤ 10 ms (data not shown).

4. Theory and discussion

4.1. Rectangular pulses

It is recalled that the SC of the skin of a subcutaneous tumor represents the highest resistance for ion motion. Therefore, the conductance relaxations in Fig. 4 refer dominantly to the SC. As shown for isolated cells and cell aggregates [18], the multiphase time course of the conductance $G(t) = I(t)/U$ of the tumor may also reflect a series of coupled processes.

Therefore, the overall relaxation curves in the presence of the field are analyzed in terms of reaction normal modes [1], i.e., as a sum of exponential terms reflecting coupled single processes. The general parameter equation for the kinetic normal modes $G_i(t)$is:

$$G(t) = \sum G_i(t) = \sum \bar{G}_i[1 - \exp(-t/\tau_i)] \quad (4)$$

where $\bar{G}_i$ is the amplitude and τ_i the relaxation time of the i-th relaxation process, respectively. Within the limits of time resolution for pulse durations in the ms range, the data in Fig. 4 are satisfactory described by the specific expression

$$G(t) = G_0 + \bar{G}_1 + \bar{G}_2[1 - \exp(-t/\tau_2)] + m_3 t \quad (5)$$

where, for the average tumor in the setup sketched in Fig. 2, the zero conductance is $G_0 = 85 \pm 56$ μS for $\ell = 0.9 \pm 0.1$ cm; number of tumors $n = 5$, one tumor per given voltage (Fig. 4). $\bar{G}_1$ is the amplitude of the first relaxation phase (here not time-resolved). The relaxation mode 2 in the presence of the field is characterized by the amplitude $\bar{G}_2$ and the time constant τ_2. The third process is represented by a so-called inclined baseline with the slope $m_3 = \bar{G}_3/\tau_3$ as the ratio of the amplitude $\bar{G}_3$ and time constant τ_3. This approximation is valid for the time range $t \ll \tau_3$, where $G_3(t) = \bar{G}_3\,[1 - \exp(-t/\tau_3)] = \bar{G}_3 \cdot t/\tau_3 = m_3 t$ holds. The conductance relaxations during the second and third pulse do not start from stationary G-values of the after-field relaxations. Therefore, the quantitative analysis of the $G(t)$ curves is here restricted to the first pulse.

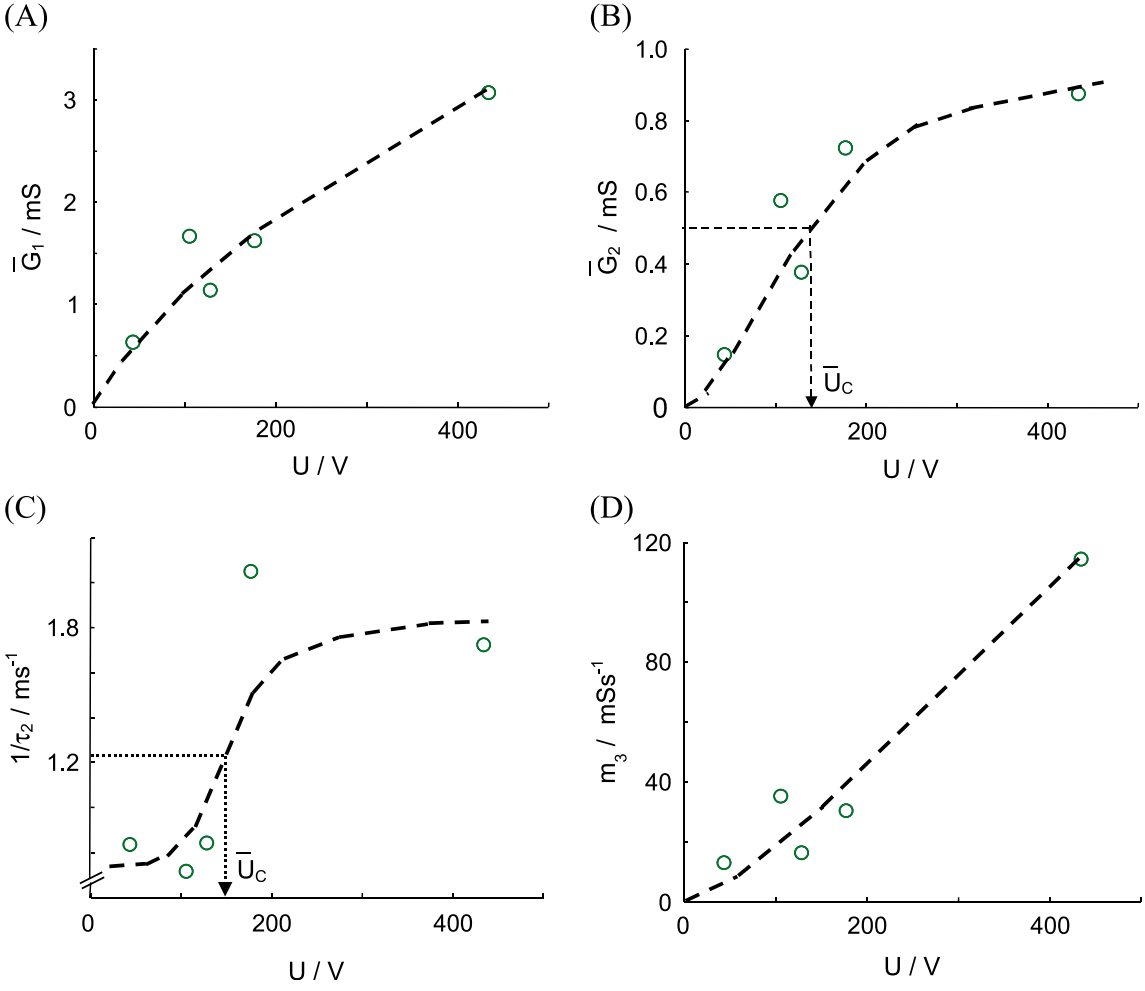

Fig. 7. The relaxation parameters $\bar{G}_1$ (A), $\bar{G}_2$ (B), $1/\tau_2$ (C) and $m_3 = \bar{G}_3/\tau_3$ (D), see Eq. (5) of the text, as a function of the voltage U, respectively. The midpoint voltage for the MEP parameters $\bar{G}_2$ and τ_2 is estimated to be the same within the margin of error: $\bar{U}_C = 130 \pm 20$ V ($\ell = 0.9$ cm) and τ_2 ($\bar{U}_C$) $= 0.7 \pm 0.1$ ms. Note that the dashed lines are drawn to illustrate the trends in the voltage dependences for these specific examples where, at the present stage of the experimental data base, a more detailed fit of the data points would not be justified. The experimental conditions are given in the legend to Fig. 4.

In Fig. 7, it is seen that all reaction normal mode quantities $\bar{G}_1$, $\bar{G}_2$, $1/\tau_2$ and m_3, respectively, increase with increasing voltage U. The amplitude $\bar{G}_1$ is suggested to reflect the formation of small, yet conductive electropores without appreciable electrolyte net transport between cell interior and the outside medium [14]. At higher field strengths, $\bar{G}_1$ may contain contributions from Wien-effects due to perturbations of ionic atmospheres and ion-pairing processes on the cell surfaces [18,26] or other processes not yet specifiable. When compared with relaxation data of salt-filled vesicles and densely packed cell aggregates, the amplitudes $\bar{G}_2$ and the relaxation rates $1/\tau_2$ exhibit the typical features, such as sigmoidal dependencies, of conductive pores [14,18]. By qualitative inspection, we obtain the midpoint voltage $\bar{U}_c(\bar{G}_2) = 130 \pm 20$ V for the mean electrode distance $\ell = 0.9 \pm 0.1$ cm, the value $\bar{G}_2(\bar{U}_c)$ and the time constant $\tau_2(\bar{U}_c) = 0.7 \pm 0.1$ ms, as derived from data of rectangular pulses of duration $t_E = 10$ ms. Because of ion flow through the larger pores the cell membranes discharge partially. Thereby the membrane field is reduced. See Eqs. (1) and (2). It is recalled that Joule heating is negligibly small up to $U = 350$ V for $\ell = 0.9$ cm used here. There are no indications of damage like burning at the electrode surfaces.

The original current trace $I(t)$ contains a capacitive contribution $I_{cap} = I^0 \exp[-t/\tau_m]$, where $\tau_m = R_m C_m$ (with $R_m = R_i$) is obtained from the impedance data. The trace is readily reproduced from Eq. (4) or Eq. (5). With Eq. (4), $I(t) = G(t)/U$ is given by $I(t) = I^0 \cdot \exp[-t/\tau_m] + G_0 U + \bar{I}_1 + \bar{I}_2 [1 - \exp(-t/\tau_2)] + \bar{I}_3(t/\tau_3)$, where I_0, $G_0 U$, $\bar{I}_1 = \bar{G}_1 U$, $\bar{I}_2 = \bar{G}_2 U$ and $\bar{I}_3$, respectively, are the additive amplitude contributions to $I(t)$. The time point t_{min} of the current minimum $I(t_{min})$ is derived from the condition $dI(t)/dt = 0$ at $t = t_{min}$. For the lower voltage range where $m_3 = \bar{I}_3/\tau_3 = 0$, we find $t_{min} = \frac{\tau_2 + \tau_m}{\tau_m - \tau_2} \ln\left(\frac{\bar{I}_2}{\tau_2} \cdot \frac{\tau_m}{I^0}\right)$. Inserting $t = t_{min}$, $I(t_{min})$ can be calculated.

The current or conductance relaxations after turning off the pulse at $t = t_E$ may be parameterized in terms of reaction normal mode quantities similar to those in the in-field relaxations. The general conductance expression for the range $t \geq t_E$ is:

$$G^{off}(t) = \sum_i G_i^{off}(t) = \sum_i \bar{G}_i^{off} \exp(-t/\tau_i^{off}) + G_\infty \qquad (6)$$

For the data in Fig. 4, Eq. (6) is specified as:

$$G^{off}(t) - G_\infty = \bar{G}_1^{off} + \bar{G}_2^{off} \exp(-t/\tau_2^{off}) + \bar{G}_3^{off} \exp(-t/\tau_3^{off}) \qquad (7)$$

where G_∞ refers to G at $t \to \infty$.

Since the time interval between the successive pulses is only 1 s (Fig. 4), Eq. (7) is here applied only to the off-field relaxations after the third pulse where within 5–6 s the parameters appearing in Eq. (7) are specified as an instructive example. The after-field parameters are displayed in Fig. 8 as a function of the voltage for $\ell = 0.9 \pm 0.1$ cm. $\bar{G}_1^{off}$ refers to the rapid resealing phase of pores without appreciable ion release during the pulse time [14]. The pairs $\bar{G}_2^{off}$, τ_2^{off} and $\bar{G}_3^{off}$, τ_3^{off}, respectively, refer to the two kinetically distinguishable, slow pore resealing processes underlying the recovery of the membrane resistance. In Fig. 8, it is seen that the after-field amplitudes $\bar{G}_1^{off}$ and $\bar{G}_2^{off}$ as well as the after-field relaxation times $\tau_2^{off} = 4 \pm 1$ s and $\tau_3^{off} = 50 \pm 5$ s change only slightly with U. Solely $\bar{G}_3^{off}$ changes considerably with U; the largest slope $d(\bar{G}_3^{off})/dU$ is associated with the midpoint voltage $\bar{U}_c$ $(\bar{G}_3^{off}) = 120 \pm 20$ V for $\ell = 0.9 \pm 0.1$ cm.

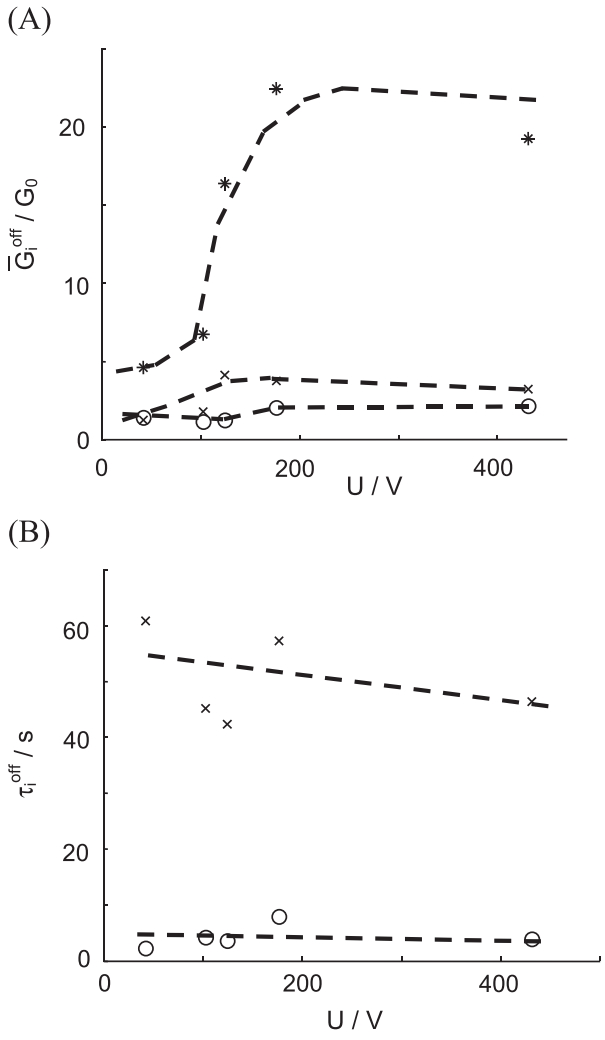

Fig. 8. The after-field relaxation parameters. (A), the kinetic normal mode amplitudes $\bar{G}_1^{off}$ (○), $\bar{G}_2^{off}$ (x), $\bar{G}_3^{off}$ (*) normalized to the conductivity $G_0 = 0.1 \pm 0.05$ mS (before electroporation) and (B) the relaxation time constants τ_2^{off} (○) and τ_3^{off} (x), as a function of the voltage of the third pulse (see Fig. 4). For $\ell = 0.9 \pm 0.1$ cm, the midpoint voltage is $\bar{U}_C$ $(\bar{G}_3^{off}) = 120 \pm 20$ V. Note that ℓ is slightly different for the n = 5 different tumors. The time intervals of one second between the first and second pulse and the second and third pulse (Fig. 4), respectively, are too short for a meaningful analysis with Eq. (7).

4.2. Trapezium pulses

Evidently, the currents $I^{\wedge}(t)$ of the three time ranges of the trapezium pulse, rising edge (r), stationary phase (s), and falling edge (f), respectively, contain capacitive and resistive contributions and reflect linear and nonlinear dependencies of the current on voltage. When compared with $\bar{U}_c(\bar{G}_2)$ and $\tau_2(\bar{U}_c)$ for rectangular pulses, Fig. 7B and C, the nonlinear contributions are in a voltage and time range, respectively, which are consistent with progressive MEP. The nonlinear contribution (without MEP) at the rising edge (r) of the trapezium is described by $I^{\wedge}_{\mathrm{nonlin}}(t) = I^{\wedge}(t) - I^{\wedge}_{\mathrm{lin}}(t)$. Explicitly,

$$I^{\wedge}_{\mathrm{nonlin}}(t) = I^{\wedge}(t) - U^{\wedge}_{\mathrm{r}}(t)/R_{\mathrm{a}} - m_{\mathrm{U}} C_{\mathrm{m}}[1 - \exp(-t/\tau_{\mathrm{m}})] \tag{8}$$

where $\tau_m = C_m R_m = C_m R_i$ and the prepulse impedance data R_a, R_a, R_i and C_m (Fig. 1) can be used.

It is seen in Fig. 9 that, above $U = 5$ V ($\ell = 1.1$ cm), $I^{\wedge}(t)$ depends nonlinearly on $U^{\wedge}(t)$. It is therefore appropriate to use the differential conductance $G_D = \mathrm{d}I^{\wedge}(t)/\mathrm{d}U^{\wedge}(t)$ for the description of the transition of G from a lower voltage range $5 < U/\mathrm{V} < 120$ to a higher voltage range $120 < U/\mathrm{V} < 500$ (Fig. 9). The transition point of the rising phase at U^*_r is obtained by fitting G_D with two linear functions, here intersecting at $U^* = U^*_r = 190 \pm 20$ V. It is interesting that U^*_r is sufficiently above the midpoint voltage $\bar{U}_c(\bar{G}_2) = 130 \pm 20$ V (Fig. 7) to cover the upper part of the range $\bar{U}_c \pm \Delta\bar{U}_c$ of effective electroporative transport. The numerical values represent characteristic parameters valid for all tumors so far measured in our setup (Fig. 2).

During the stationary phase (s), where the voltage is kept constant, the further increase in the current, solid current line (Fig. 6), suggests continuation of pore formation and partial discharging of cell membranes as well as Joule heating. The current contribution due to Joule heating, which is caused by the higher current density due to pore formation, is described by:

$$\Delta I^{\wedge}_{\mathrm{J}}(t) = I^{\wedge}_{\mathrm{S}}(t) - I^{\wedge}_{\mathrm{S,corr}}(t) = \Delta G_{\mathrm{J}}(t) \cdot U^{\wedge}_{\mathrm{S}} \tag{9}$$

The respective conductance contribution is:

$$\begin{aligned}\Delta G_{\mathrm{J}}(t) &= G_{\mathrm{S}}(t) - G_{\mathrm{S,corr}}(t) \\ &= G_{\mathrm{S}}(t) \cdot k_{\mathrm{J}} \cdot \Delta T(t)/[1 + k_{\mathrm{J}} \cdot \Delta T(t)]\end{aligned} \tag{10}$$

where the familiar relationship $G_s(t) = G_{\mathrm{S,corr}}(t)/[1 + k_J \cdot \Delta T(t)]$ is applied. This contribution is very significant for higher voltages (U>300 V) and can be estimated using the temperature coefficient, for instance, of 0.1 M KCl solution (modeling the cell interior): $k_J = 0.026\ \mathrm{K}^{-1}$ at $T = 298$ K (25 °C). The temperature increase may be calculated according to

$$\Delta T(t) = U^{\wedge}_{\mathrm{S}} \int I^{\wedge}_{\mathrm{S}}(t) \cdot \mathrm{d}t/C \approx U^{\wedge}_{\mathrm{S}} \sum I^{\wedge}_{\mathrm{S}}(t)\ \Delta t/C \tag{11}$$

where $C = \rho c_p \cdot \ell_{\mathrm{eff}} \cdot A_{\mathrm{eff}}$ is the heat capacity of the tissue and Δt is an adequately chosen small time interval between the individual $I^{\wedge}_S(t)$ values. The tissue mass density ρ and the tissue specific heat capacity c_p may be approximated by $\rho(H_2O)$ and $c_p(H_2O)$ of water at 298 K, respectively.

The corrected current contribution $I^{\wedge}_{\mathrm{S,corr}}(t)$, Eq. (9), in the phase (s), dashed current line (Fig. 6), heading at $I_{\mathrm{max,corr}}$ is described by:

$$\begin{aligned}I^{\wedge}_{\mathrm{S,corr}}(t) &= (I_{\mathrm{max,corr}} - I_{\mathrm{r,E}})[1 - \exp(-t/\tau_{\mathrm{S}})]\ + I_{\mathrm{r,E}} \\ &= G_{\mathrm{S,corr}}(t) \cdot U^{\wedge}_{\mathrm{S}}\end{aligned} \tag{12}$$

where τ_S is the time constant of the corrected current relaxation. Applying now the Eqs. (9) to (12) to the data in Fig. 6, yields the time constant $\tau_S = 0.6 \pm 0.2$ ms and the amplitude $\bar{G}_{\mathrm{S,corr}}$ according to

$$G_{\mathrm{S,corr}}(t) = \bar{G}_{\mathrm{S,corr}}[1 - \exp(-t/\tau_{\mathrm{S}})]. \tag{13}$$

In Fig. 10, the conductance $G_f(t) = I^{\wedge}_f(t)/U^{\wedge}_f(t)$ of the falling edge (f) decreases in roughly two phases. The $G_f(t)$ relaxation may be approximated by the two linear voltage ranges $0 < U^{\wedge}_f < U^*_f$ and $U^{\wedge}_f > U^*_f$, respectively. It is suggested to use the estimate of $U_{\mathrm{off}} = U^*_f = 70 \pm 10$ V for $\ell = 0.7$ cm as the characteristic voltage at which sufficiently many electropores remain permeable for further small-ion transport and most likely also for the electrophoretic transport of larger ionic molecules like DNA or proteins. It is recalled that the data given in (Figs. 6, 9, and 10), respectively, are illustrative examples, out of 15 tumors measured and quantitatively analyzed.

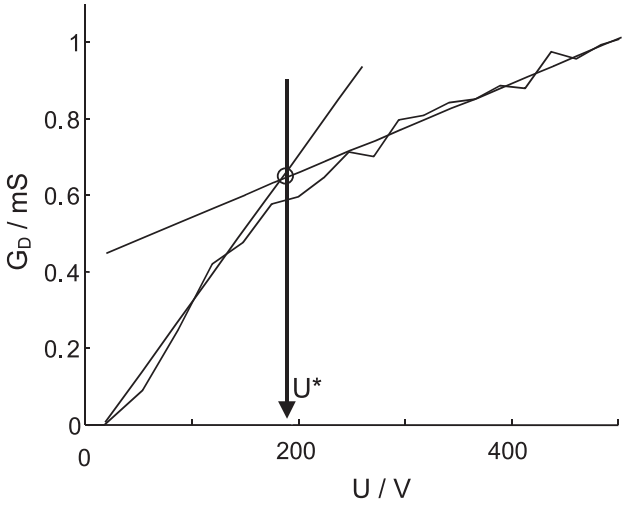

Fig. 9. The differential conductance $G_D = \mathrm{d}I^{\wedge}(t)/\mathrm{d}U^{\wedge}(t)$ as a function of voltage U. The transition voltage U^*_r is the voltage $U^* = 190 \pm 20$ V ($\ell = 1.1$ cm) at the intersection, obtained by fitting two linear functions to the low and the high voltage region, respectively.

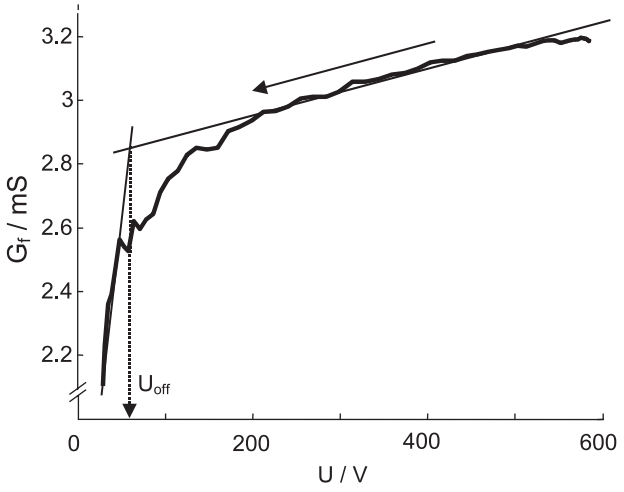

Fig. 10. The conductance $G_f^{\wedge}(U) = I_f^{\wedge}(t)/U_f^{\wedge}(t)$ of the trapezium phase (f) as a function of U(t); see Fig. 6. The voltage $U_{off} = 70 \pm 10$ V ($\ell = 0.7$ cm) at the intersection point of the two fitting lines is U_f^*, where a major fraction of electropores returns to nonconductive states. The arrow represents the direction of the conductance decrease (falling edge) with time.

4.2.1. Practical guidance for presetting high voltage pulse generators

It is recalled that the sigmoid behavior of $\bar{G}_2(U)$, as shown in Fig. 7B, and of $1/\tau_2$, Fig. 7C, is characterized by the midpoint voltage $\bar{U}_C$, which quantifies the voltage range $\bar{U}_C \pm \Delta\bar{U}_C$ for practical applications of rectangular pulses. However, $\bar{U}_C$ as the sole parameter is not practicable for the quantification of optimum pulsing conditions, because the application of several consecutive pulses at different voltages will considerably change the passive electrical behavior of the tumor. On the other hand, the trapezium pulse data provide the estimates for rectangular pulse parameters $U_{app} \geq \bar{U}_c(\bar{G}_2)$ and $t_E = 10 \cdot \tau_2(\bar{U}_c)$, see Fig. 7. Note that an exponential change gets practically stationary at $t = 10 \cdot \tau_2$. Additionally, a minimum value of the voltage is estimated for subsequent low-voltage pulses supporting electromigration of ionic macromolecules through long-lived electroporated membrane parts.

It is recalled that the application of a time-varying voltage (ramp) yields the differential conductance $G_D = dI^{\wedge}(t)/dU^{\wedge}(t)$ as a function of voltage and time, where in our case the values for voltages below 5 V are neglected (Fig. 9). It is repeated that data fit in Fig. 9 with two linear functions of the rising phase (r) provides the characteristic quantity $U^* = U_r^*$ and the $(I^{\wedge}/U^{\wedge})_r$ characteristics of the tissue between the electrodes.

The voltage U_{app} for a rectangular high voltage pulse is chosen according to $U_{app} \geq U^*$ (Fig. 9). The maximum current at the selected voltage U_{app} and the pulse duration t_E is given by

$$I_{max}(U_{app}, t_E) = I^{\wedge}(U_{app}) + \bar{G}_{S,corr} \cdot U_{app} + \Delta G_J(t_E) \cdot U_{app}, \quad (14)$$

where the current level $I^{\wedge}(U_{app})$ is the current $I^{\wedge}(t')$ which corresponds in Fig. 6 to the selected voltage level $U^{\wedge}(t') = U_{app}$. Obviously, the time point t' in Fig. 6 is in the range $2 \leq t'/\text{ms} \leq 6$, which is the range of the ramp duration. It is recalled that this range is suggested by the relaxation data displayed in (Figs. 4, 7, and 8). Additionally, in Eqs. (10) Eqs. (11) Eqs. (12) Eqs. (13) the practical condition $t_E \approx 10\tau_S$ has been used. Note that τ_s and $\bar{G}_{S,corr}$ are defined by Eqs. (12) and (13), respectively. Since it has been found that the trapezium quantity τ_s corresponds to τ_2 of the relaxation process 2 according to $G_2(t) = \bar{G}_2[1 - \exp(-t/\tau_2)]$, Fig. 7C, the actual current $I(t_E)$ at t_E of a rectangular pulse of voltage U_{app} is calculated using the relationship:

$$I(t_E) = U_{app}\left[G(U_{app}) + (\bar{G}_{S,corr})[1 - \exp(-t_E/\tau_S)] + \Delta G_J(t_E)\right] \quad (15)$$

where $G(U_{app}) = I(U_{app})/U_{app} = I_r^{\wedge}(t)/U_r^{\wedge}(t)$ at $U_r^{\wedge}(t) = U_{app}$ is obtained from the rising phase of the trapezium pulse (Fig. 6). The stationary phase yields τ_S. We propose to specify the correspondence between τ_2 and τ_S by the approximation $\tau_2 = \tau_S$. The Joule heating correction term $\Delta G_J(t_E)$ is obtained by using the explicit relationship:

$$\begin{aligned}\Delta G_J(t_E) &= (G(U_{app}) + \bar{G}_{S,corr})[(1 + k_J \Delta T(t_E)] \\ &= (G(U_{app}) + \bar{G}_{S,corr})[1 + k_J C U_{app}^2 (G(U_{app}) \\ &\quad + \bar{G}_{S,corr}) t_E]. \end{aligned} \quad (16)$$

Because in a rectangular voltage pulse the current contribution of the relaxation phase i is practically stationary at $t = 10\tau_i$, we suggest to preset the high voltage pulse duration as $t_E = 10 \cdot \tau_2(\bar{U}_C) = \tau_S$, to ensure successful electroporation with only small side effects.

The current at the falling edge $I_f^{\wedge}(t)$ of the trapezium pulse is treated similarly as $I_r^{\wedge}(t)$ of the phase (r), yielding $U_{off} = U_f^*$ (Fig. 10). Since the resistance after the pulse recovers rapidly (ms time range) only at $U < U_f^*$ [27], indicating rapid restoration of membrane barrier functions, the condition $U > U_f^*$, has to be applied to meet the system in the longer lasting permeabilized states produced in the previous high voltage pulse. Therefore, in those cases where the high voltage (HV)-induced transport can be enhanced by subsequent low-voltage (LV) pulses [28,29], $U_{app}(LV) \geq U_f^*$ is the voltage proposed for the LV-pulses, following the electroporation high voltage (HV) pulse. Practically, the upper current level for the termination of the HV-pulse is set to $I_{max}(U_{app}, t_E)$; see Eq. (14). If during MEP, I_{max} is reached, the pulse generator is suggested to be switched to the preset low voltage $U(LV) \geq U_f^*$. In any case, the diagnostic trapezium pulse, as a first electroporation pulse causing longer lived pore states, also conditions the tissue such that subsequent therapeutic pulses are more effective.

5. Conclusion

Based on a comparison of the current voltage characteristics (IUC) of rectangular voltage pulses with increasing voltage with that of a trapezium shaped voltage pulse, it is proposed to use the IUC of a trapezium high voltage pulse for parameter presetting on the pulse generator. The data show that voltage and time parameters obtained from the nonlinear current–voltage region of the trapezium pulse are suited to preset the high voltage (HV) and the duration t_E of the rectangular pulse to be applied in clinical electroporators for the electrotransfer of drugs and genes. The quantities calculated from the trapezium prepulse are the voltage U_r* (rising phase), characterizing MEP, and the voltage U_f* (falling phase), characterizing the resealing of the previously induced electropores, as well as the time constant τ_S of the corrected current relaxation (Eq. (12)) of the stationary phase (s) of the trapezium voltage. The pulse time t_E for the rectangular HV-pulse (and the number of pulses) has to be adjusted according to $\tau_S \approx \tau_2(\bar{U}_C)$, such that $t_E = 10\tau_S$ to provide effective electroporation and electrotransport. In the case of HV-pulsing applied to mouse skin tumors, the trapezium procedure yields the *lower* limits of the voltage and the time constant of a rectangular pulse, necessary to electropermeabilize the stratum corneum of the subcutaneous tumor. In summary, the trapezium method yields pulse parameters which, as judged from the comparison with rectangular pulse data, are useful for the presetting of the pulse voltages and pulse durations for biotechnological and medical purposes.

Acknowledgements

We gratefully acknowledge support of the Fonds Chemie, Frankfurt, the European Union (Brüssel) for Grant QLK3-CT-1999-00484 and the Deutsche Forschungsgemeinschaft for Grants Ne227/9-3 and 9-4 to E.N.

References

[1] E. Neumann, The relaxation hysteresis of membrane electroporation, in: E. Neumann, A. Sowers, C. Jordan (Eds.), Electroporation and Electrofusion in Cell Biology, Plenum Publishing Corporation, New York and London, 1989, pp. 61–81.
[2] J.C. Weaver, Electroporation: a general phenomenon for manipulating cells and tissue, J. Cell. Biochem. 51 (1993) 426–435.
[3] M. Okino, H. Mohri, Effects of a high-voltage electrical impulse and an anticancer drug on in vivo growing tumors, Jpn. J. Cancer Res. 78 (1987) 1319–1321.
[4] L.M. Mir, L.F. Glass, G. Sersa, J. Teissie, C. Domenge, D. Miklavcic, M. Jaroszeski, S. Orlowski, D.S. Reintgen, Z. Rudolf, M. Belehradek, M. Gilbert, M.P. Rols, J. Belehradek, J.M. Bauchaud, R.C. DeConti, B. Stabuc, M. Cemazar, P. Coninx, R. Heller, Effective treatment of cutaneous and subcutaneous malignant tumors by electrochemotherapy, Br. J. Cancer 77 (1998) 2336–2342.
[5] S. Orlowski, L.M. Mir, Cell electropermeabilization: a new tool for biochemical and pharmacological studies, Biochim. Biophys. Acta 1154 (1993) 51–63.
[6] M.R. Prausnitz, U. Pliquett, R. Langer, J.C. Weaver, Rapid temporal control of transdermal drug delivery by electroporation, Pharm. Res. 11 (1994) 1834–1837.
[7] E. Neumann, M. Schaefer-Ridder, Y. Wang, P.H. Hofschneider, Gene transfer into mouse lyoma cells by electroporation in high electric fields, EMBO J. 1 (1982) 841–845.
[8] K. Kinosita, T.Y. Tsong, Voltage-induced conductance in human erythrocyte membranes, Biochim. Biophys. Acta 554 (1979) 479–497.
[9] I.G. Abidor, A.I. Barbul, D.V. Zhelev, P. Doinov, I.N. Bandrina, E.M. Osipova, S.I. Sukharev, Electrical properties of cell pellets and cell electrofusion in a centrifuge, Biochim. Biophys. Acta 1152 (1993) 207–218.
[10] E. Neumann, K. Toensing, S. Kakorin, P. Budde, J. Frey, Mechanism of electroporative dye uptake by mouse B cells, Biophys. J. 74 (1998) 98–108.
[11] E. Neumann, S. Kakorin, I. Tsoneva, B. Nikolova, T. Tomov, Calcium-mediated DNA-adsorption to yeast cells and kinetics of cell transformation by electroporation, Biophys. J. 71 (1996) 868–877.
[12] E. Neumann, S. Kakorin, K. Toensing, Membrane electroporation and electro-mechanical deformation of vesicles and cells, Faraday Discuss. 111 (1998) 111–125.
[13] E. Neumann, S. Kakorin, Digression on membrane electroporation for drug and gene delivery, Techn. Cancer Res. Treat. 1 (2002) 329–339.
[14] T. Griese, S. Kakorin, E. Neumann, Conductometric and electrooptic relaxation spectrometry of lipid vesicle electroporation, Phys. Chem. Chem. Phys. 4 (2002) 1217–1227.
[15] K.S. Cole, Membranes, Ions and Impulses, University of California Press, Berkeley, USA, 1968.
[16] M. Hibino, H. Itoh, K. Kinosita, Time courses of cell electroporation as revealed by submicrosecond imaging of transmembrane potential, Biophys. J. 64 (1992) 1789–1800.
[17] E. Tekle, R.D. Astumian, W.A. Friauf, P.B. Chock, Asymmetric pore distribution and loss of membrane lipid in electroporated DOPC vesicles, Biophys. J. 81 (2001) 960–968.
[18] M. Schmeer, Elektroporation von Zellpellets als Gewebemodell, PhD Thesis (2003), University of Bielefeld..
[19] U. Pliquett, R. Vanbever, J.C. Weaver, Local transport regions (LTRs) in human stratum corneum due to long and short high voltage pulses, Bioelectrochem. Bioenerg. 47 (1998) 151–161.
[20] U. Pliquett, R. Langer, J.C. Weaver, Changes in the passive electrical properties of human stratum corneum due to electroporation, Biochim. Biophys. Acta 1239 (1995) 111–121.
[21] S. Kakorin, S.P. Stoylov, E. Neumann, Electrooptics of membrane electroporation in diphenylhexatriene-doped lipid bilayer vesicles, Biophys. Chemist. 58 (1996) 109–116.
[22] U. Pliquett, T.E. Zewert, T. Chen, R. Langer, J.C. Weaver, Imaging of fluorescent molecule and small ion transport through human stratum corneum during high-voltage pulsing: localized transport regions are involved, Biophys. Chemist. 58 (1996) 185–204.
[23] E. Neumann, Membrane electroporation and direct gene transfer, Bioelectrochem. Bioenerg. 28 (1992) 247–267.
[24] U. Pliquett, Non linear current voltage characteristics of biological matter, in: S. Grimnes, O.G. Martinsen, H. Bruvoll (Eds.), Proceedings Intern. Conf. on Electrical Bio-Impedance, 26.6.–29.6, University Press, Oslo, Norway, 2001, pp. 39–42.
[25] R. Elez, A. Piper, B. Kronenberger, M. Kock, M. Brendel, E. Pliquett, U. Pliquett, E. Neumann, S. Zeuzem, Tumor regression by combination antisense therapy against Plk1 and Bcl-2, Oncogene 22 (2003) 69–80.
[26] Z.A. Schelly, R.D. Astumian, A theory for the apparent "negative second Wien effect" observed in electric-field-jump studies of suspensions, J. Phys. Chem. 88 (1984) 1152–1156.
[27] U. Pliquett, M. Schmeer, T. Seipp, E. Neumann, Fast recovery process after electroporation, Int. Fed. Med. Biol. Eng. Bioimpedance 2 (2002) 98–99.

[28] S.I. Sukharev, V.A. Klenchin, S.M. Serov, L.V. Chernomordik, Y.A. Chizmadzhev, Electroporation and electrophoretic DNA transfer into cells. The effect of DNA interaction with electropores, Biophys. J. 63 (1992) 1320–1327.
[29] L.M. Mir, M.F. Bureau, J. Gehl, R. Rangara, D. Rouy, J.-M. Caillaud, P. Deleare, D. Branellec, B. Schwartz, D. Scherman, High-efficiency gene transfer into skeletal muscle mediated by electric pulses, Proc. Natl. Acad. Sci. U. S. A. 96 (1999) 4262–4267.

Glossary

a: cell radius
A_{eff}: effective area of the electrode
C_m, R_m: overall capacitance and resistance of cell membranes, respectively
d_m: thickness of the cell membrane
E: electric field strength
$\bar{E}_c$, $\bar{E}_c(\bar{G}_2)$: midpoint field strength, midpoint field strength of $\bar{G}_2$of phase (2)
E_{ind}: induced membrane field strength
E_m: membrane electric field strength
G, R: conductance, resistance, respectively
G_0: dc conductivity before pulse application
$\bar{G}_I$: reaction normal mode conductance amplitude of phase i (voltage step)
G_D: differential conductance
$\bar{G}_i^{off}$: normal mode amplitude of relaxation phase i after the pulse
I_{max}: maximum current of preset rectangular pulse (U_{app}, t_E)
$I_{max,corr}$: corrected maximum current for the trapezium voltage phase $U_S^{\wedge}$
$I_{r,E}$: current at the end of the rising edge (r)
$I^{\wedge}(t)$: current of the trapezium voltage pulse
$I_S^{\wedge}(t)$: current at the steady state voltage $U_S^{\wedge}$ of the trapezium pulse
$I_f^{\wedge}$, $U_f^{\wedge}$: current and voltage at the trapezium falling edge (f), respectively
LTR: localized transport regions
ℓ, ℓ_{eff}: distance and effective distance between the plate electrodes, respectively
t_E: duration of rectangular pulse
U_{app}: voltage applied at the outer electrodes
U_r^*: voltage of the rising phase at the intersection point (U*, Fig. 9)
U_f^*: voltage of the falling phase at the intersection point (U_{off}, Fig. 10)
$\bar{U}_C$, $\bar{U}_C(\bar{G}_2)$: midpoint voltage, midpoint voltage for $\bar{G}_2$, respectively
$\Delta\varphi_{ind}$: induced transmembrane potential
$\Delta\varphi_{nat}$: natural membrane potential
κ_m, κ_{ex}, κ_{in}: conductivity of the membrane, external and internal medium, respectively
τ_I: time constant of the relaxation phase i
τ_m: time constant of the capacitive relaxation contribution